



Impact of Melt Flow and Surface Tension on Gap Bridging During Laser Beam Welding

Joerg Volpp¹ 

Accepted: 17 July 2023 / Published online: 26 July 2023
© The Author(s) 2023

Abstract

Laser beam welding is an essential technology to enable the transformation to enforce e-mobility. When manufacturing light weight structures like the chassis, precision, speed, quality and low deformation can be expected when using the laser beam as a welding heat source. However, the laser beam is typically used at small dimensions and can fail to transfer its energy to the joining partners when the gap between them becomes large. Beam shaping technologies have developed in the last years to be flexibly used for high-power processes and provide an opportunity to alter the energy input and thereby improve the welding quality and gap bridgability. In this work, multi-spot beam shaping was analyzed using up to nine spots. Experiments were performed using different beam shapes in order to redistribute the energy input, recording the process using high-speed imaging for detection of melt pool dimensions. Those were used as input for a simplified analytical model predicting the process collapse based on the available melt material. Several beam shapes created melt pools that support the material availability behind the keyhole(s). Numerical simulations showed that directed melt flows induced by the keyhole(s) can increase the gap bridgability.

Keywords Keyhole Welding · Fluid Flow · Modelling · Simulation · Gap Bridging

✉ Joerg Volpp
jorg.volpp@ltu.se

¹ Department of Engineering Sciences and Mathematics, Luleå University of Technology, Luleå 97187, Sweden

Introduction

Motivation

In order to enable the conversion to e-mobility, many challenges have to be overcome. One aspect is the efficient design of vehicles regarding their weight. Lightweight design manufacturing requires precise production methods that enable the required structures. One critical component is the vehicle chassis. Due to safety reasons, the chassis must resist a manifold of loads and impacts but should be lightweight in order to minimize the energy consumption during vehicle use. Lightweight chassis designs are driven by using light materials and smart design shapes. Those structural parts need to be joined during the manufacturing to form the complete chassis structure.

Typically, welding is used to create the necessary material bonding. Conventional welding using arc processes often require joint preparation and the application of additional material, which is often a processing challenge [1]. More important, the arc processes induce extensive heat input into the joining partners, which can lead to significant residual stresses and deformations. The shrinkage of the weld seam during cooling and the angular deformations can result in problems when adding further chassis elements. In particular, the gaps between the joining elements can increase, which can alter or stop a joining process [2].

The use of a laser beam as energy source can significantly reduce the deformation due to the minimum and directed heat input, limit the joint preparation, and increase the productivity due to the rapid processing. However, the laser beams typically used for welding are comparably small (often < 1 mm, typically around $300\ \mu\text{m}$, [3]). Therefore, the laser beam welding process with typical single spot arrangements are sensitive to gaps between the joining partners. In worst case, the laser beam can miss the material completely, when the gap is larger than the laser beam dimension. Complex clamping procedures can help to keep the joining partners in place and guarantee small gap sizes [4] but can require much effort and limit the flexibility of the otherwise flexible tool laser. Another way of overcoming this challenge is to increase the illumination area of the laser beam by beam shaping.

Beam Shaping

Laser beam shaping is used already for many decades. In laser hardening, line or rectangular shapes were created using oscillating beams [5], refractive [6] and even diffractive optics [7] or kaleidoscopes [8] in order to enlarge the treatable area. For laser beam brazing, additional laser spots ahead of the actual processing beam were shown to enable coating removal and a better wetting behaviour. In laser beam welding, dynamic beam shaping using oscillation optics were used to enable joining of hard-to-weld materials, e.g. copper [9]. Multi-spot welding was demonstrated to increase the process stability. Spot-in-spot techniques showed for example a more stable keyhole [10]. Diffractive static beam shaping enables nowadays the creation of almost all kinds of beam shapes at high laser power. Refractive beam shaping of tophat and donut profiles was shown to be able to alter the keyhole shapes and the spatter and pore formation due to the altered dynamic keyhole oscillations and smoother vapor

outflow [11]. However, beam shaping can also create multiple spots with variable laser power. Those can be positioned along the laser beam axis [12] or next to each other. Bi-focus welding was shown to reduce the number of spatters [13]. It was seen that using multiple laser spots, it is possible to create complex keyholes with varying impact on the melt flow patterns [14]. Up to nine spots were shown to be able to create complex, but promising process conditions [15].

Surface Tension and Melt Flow

The melt pool behaviour depends also on the melt pool temperature induced by the heat input by the laser beam. The melt pool forms based on heat conduction and multiple reflections inside the keyhole (e.g. [16].). Melt pool surfaces form according to the surface tension and show the typical rounded shapes. The surface tension is, however, temperature dependent. Therefore, the surface tension is (for most materials) higher at low temperatures, which induces surface melt movement, known as Marangoni flow (e.g. [17].). In general, the surface tension tries to form round surface shapes, which means that when welding different sheets, the material bridging the gap has the tendency to favour the accumulation on the sheets. The melt flow in keyhole welding can be quite complex. In general, the melt is accelerated when passing the keyhole and creates a dynamic melt pool behind the keyhole [18]. It was seen that those melt movements can be influenced by process and material parameters [19].

It is not yet clear, how the altered energy input induced by beam shaping impacts the melt flow and if such a melt flow can be used to support the melt bridge between the joining partners in laser beam welding. Therefore, in this work, gap bridging with different beam shapes was investigated to help to explain the phenomena that promises to increase the gap bridgability.

Materials and Methods

Opening Gap Experiments

A multi-mode fibre laser (IPG, maximum power output 15 kW) was used for the experiments. The laser beam was used in focal position and slightly inclined (7°) to avoid back-reflections into the fibre. A power of 3 kW at a welding speed of 3 m/min and Argon shielding through a side-gas nozzle at 18 L/min was applied for all experiments.

In order to evaluate the gap bridgability, an opening gap experiment was set up (Fig. 1). DP800 material of 1.1 mm thickness was used. The laser beam was moved from the practical zero-gap along the 100 mm long sheets that showed a gap of 0.6 mm at the end of the welding process. The gap width at failure was extracted as a measure of gap bridgability [14].

During the welding, a high-speed camera (Photron) was used to visualize the processing zone at a recording frame rate of 4000 fps in combination with an illumination system (Cavitar). From the videos, the melt pool lengths and widths were measured.

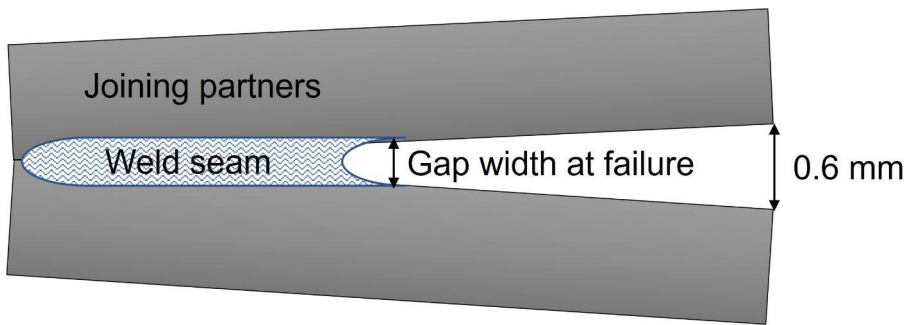


Fig. 1 Sketch of a top view of the opening gap experiment (the laser beam was moving from left to right)

Beam Shapes

Refractive beam shaping optics were used to form various multi-spot beam shapes. The quattroXX optic (Adloptica, Berlin, Germany) gives up to four separate laser spots in a square of is 0.68×0.68 mm using a 150 mm collimator and 250 mm focusing lens. The peaXXus optic (Adloptica, Berlin, Germany) gives a square of 0.45×0.45 mm with up to nine spots. Each single spot has a diameter of ~ 200 μm . The analyzed beam profiles and related high-speed images are shown in Fig. 2.

Melt Pool Appearance Calculations

In order to model the circumstances that can lead to a break-up of the melt bridge between the joining partners during welding, a simplified analytical model was developed. The model considers the melt pool dimensions (extracted from high-speed images) and predicts the keyhole height based on surface tension effects in the melt pool.

The available material A_{melt} and volume V_{melt} for creating the melt pool was calculated as the cross-sectional area and along the melt pool length l , respectively (Fig. 3a) to

$$\begin{aligned} A_{melt} &= (s - g) \cdot t \\ V_{melt} &= A_{melt} \cdot l \end{aligned} \quad (1)$$

with the melt pool width s , the gap width g and the sheet thickness t .

The melt pool surface height h (yellow line in Fig. 3) was assumed to follow a logarithmic curve from behind the keyhole to the rear of the melt pool along the melt pool length l as a fit from high-speed imaging observations of the melt pool surface.

$$h(l) = 0.1 \cdot \ln(l) + 0.4 \quad (2)$$

Since the main acting force on the melt pool surface behind the keyhole is the surface tension, the local curvature of the melt pool surface along the melt pool length and

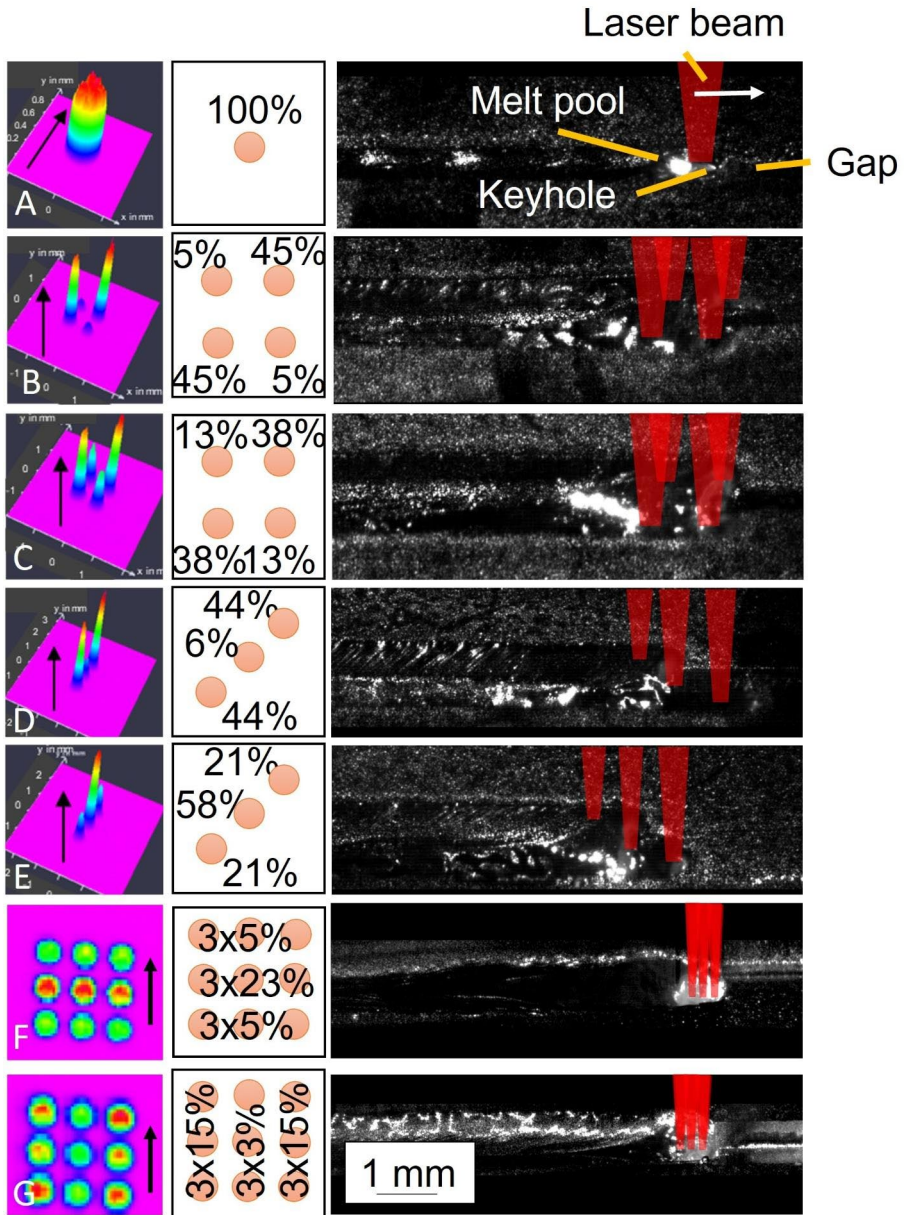


Fig. 2 Used beam shapes and high-speed images showing the processing zones and created tracks

width must be equal in value with different curvature to form a stable system (Young-Laplace equation):

$$\frac{\gamma}{R_1} = -\frac{\gamma}{R_2} \quad (3)$$

with the surface tension γ of the material and the radii of the two curvatures R_1 and R_2 both denoted to R (Fig. 3b).

The area A (Fig. 3b) was calculated along the melt pool length with the circle length b to

$$A = \frac{R \cdot b}{2} - \frac{s \cdot (R - h)}{2} \quad (4)$$

The total area was derived by integrating along the melt pool length dl and compared to the available melt volume V_{melt} . The remaining keyhole height k was derived in case enough material is available to establish a keyhole to

$$k = h_{(l=0)} \quad (5)$$

Numerical Melt Flow Analysis

A numerical fluid-dynamic model was developed to simulate the temperature field and melt flow characteristics when using different beam shapes. The keyhole dimensions were extracted from the high-speed images and the keyhole was inserted as a cylinder into the computation domain, penetrating the whole sheet (Fig. 4).

Mesh refinement was used around the keyhole in order to resolve the expected high thermal gradients and fast melt flows. The material was modelled as a fluid with high viscosity moving through the computational domain at the welding speed. The material was assumed to be pure iron. When the melting temperature is reached,

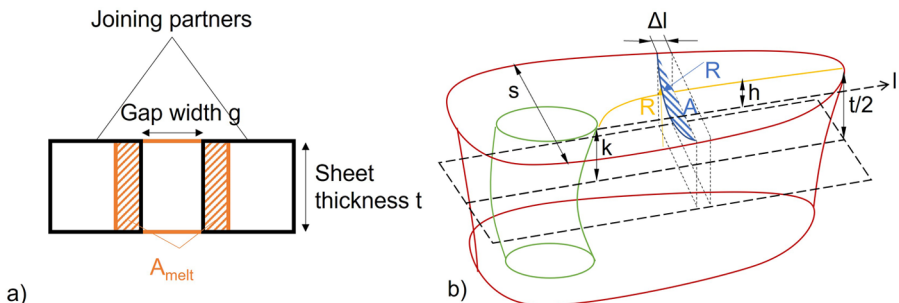


Fig. 3 Sketches of (a) the cross-section of the joining partners and (b) the melt pool including keyhole and geometrical dimensions for the calculations

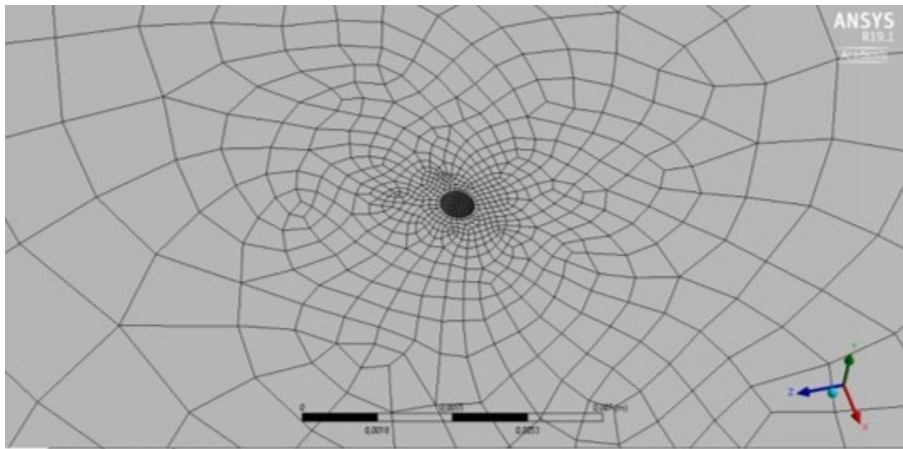


Fig. 4 Top view of the computational domain including the keyhole and the mesh

the viscosity is set to the real material viscosity and gravity and Marangoni effects are considered to model the melt flow. The ANSYS CFX solver was used for the simulations. The model was validated comparing cross-sectional melt pool dimensions from the simulation and the shape of the re-melted areas in cross-sections from experiments.

All process parameters were chosen as used in the experiments. No gas flow was assumed. The energy input was modelled using volumetric heat sources with Gaussian profiles, using one profile for the single spot welding and multiple spots arranged according to the experimental possibilities. Both temperature distributions and melt flow patterns were extracted from the simulation results.

Results

Gap Bridgability

The gap width at failure during the opening gap experiments were evaluated (Fig. 5). All process results using shaped beams show a higher gap bridgability compared to the single spot beam process (A). Beam shape F showed the largest gap bridgability.

Melt Pool Dimensions

Melt pool dimensions were extracted from the high-speed images (Fig. 6). When using four or more spots, the melt pool length can be very high. At shapes B and C, also the melt pool width is comparably high, while at nine-spot welding (shapes F and G), the melt pool width remains comparably low.

From the analytical calculations, the remaining keyhole heights were derived (Fig. 7). Beam shapes A and D show no remaining keyhole height, which means that

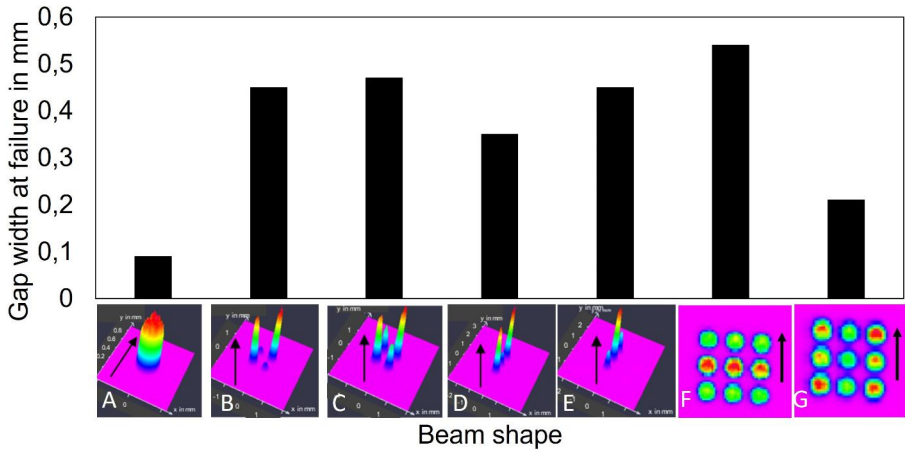


Fig. 5 Gap width at failure measured in opening gap experiments

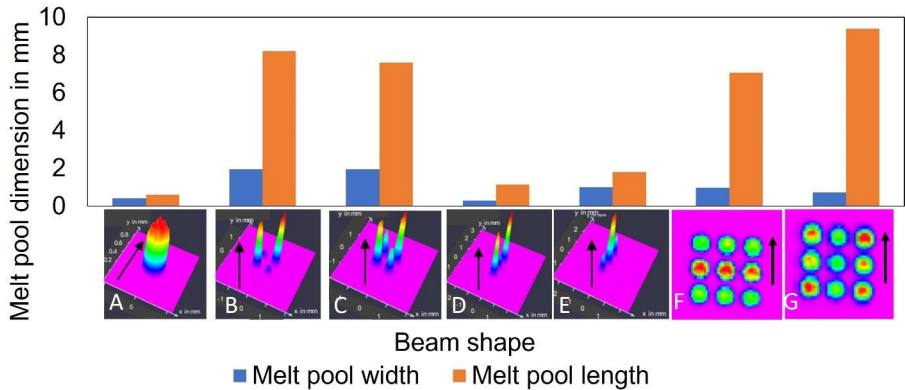


Fig. 6 Melt pool width measurements from high-speed images

the keyhole rear wall must be shifted from its intended position due to the lack of molten material. The four-spot profiles show the highest remaining keyhole heights.

Melt Flow Simulations

The fluid dynamic simulation was performed with a single beam and a four-beam arrangement (Fig. 8). At single spot welding, the temperature is concentrated on the keyhole front area and the flow field shows turbulent characteristics. The trajectories show a flow away from the central melt pool behind the keyhole. For the four-beam arrangement, the trajectories smoothly combine behind the keyhole and remain in this position.

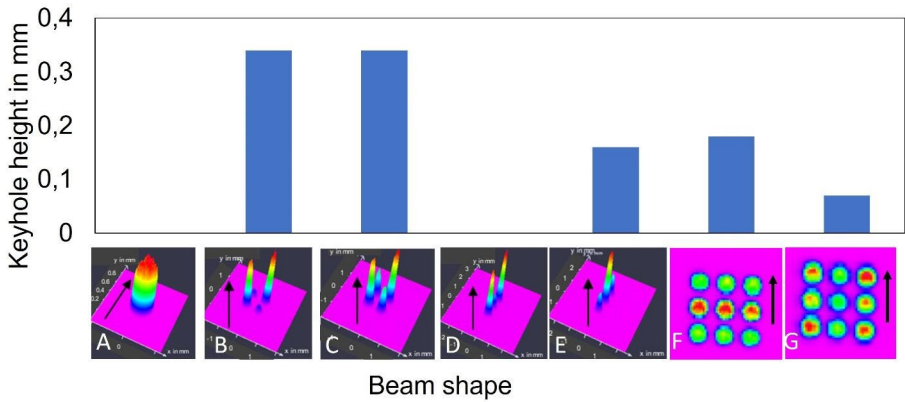


Fig. 7 Calculated remaining keyhole height at different beam shapes

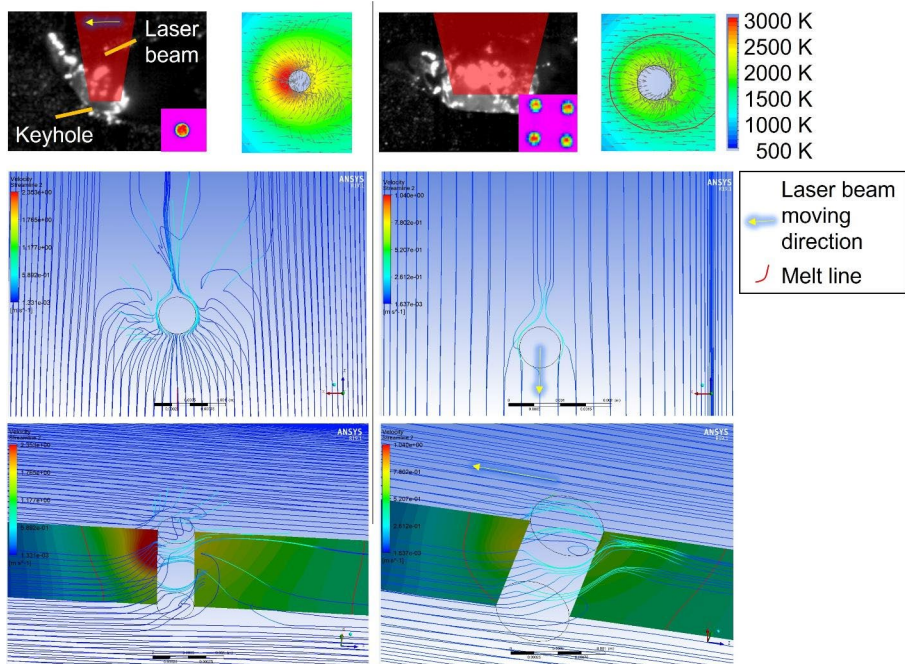


Fig. 8 Examples of thermal and melt flow visualizations (left: beam shape A; right: beam shape: C)

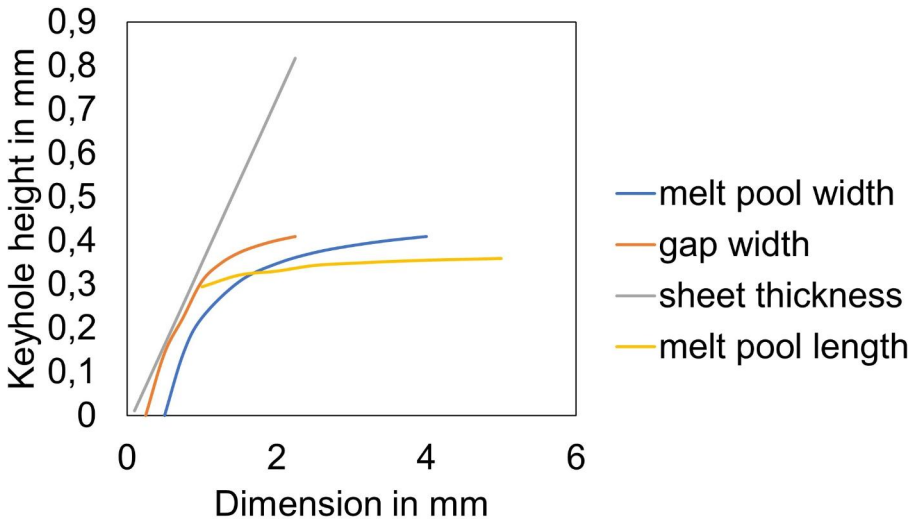
Discussion

A calculation was performed using the simplified analytical model in order to analyse the effects of single parameters on the keyhole height. The calculation was based on the parameters given in Table 1, while one of the parameters was varied (Fig. 9).

At small melt pool widths and large gap widths a keyhole collapse was calculated. In the calculated range, the sheet thickness and melt pool length did not lead to a

Table 1 Parameters used for the calculations

Dimension	Value	Unit
Melt pool width s	2	mm
Gap width g	0.5	mm
Sheet thickness t	1	mm
Melt pool length l	3	mm

**Fig. 9** Keyhole height calculation when varying single parameters in the analytical model

keyhole collapse. At increasing gap widths, the available material is reduced and at decreasing melt pool widths, the surface tension leads to steep melt pool surface shapes, which cannot create a keyhole anymore.

Beam shapes B and C result in both high gap bridgability and high keyhole heights, while profile A shows low values. This is an indicator that the simplified model shows reasonable outcome and that the melt availability in combination with surface tension effects have a significant effect on the gap bridgability. Beam shape D shows comparably good gap bridgability but should not have enough material to form a stable keyhole. Also beam shapes E, F and G should have less material available, but show good gap bridgability.

One possible reason for this effect can be the melt flow. The melt pool is highly dynamic and shows partly high-speed melt movement [18] within the melt pool. The numerical calculations of this work show that it is possible that the melt flows show different flow patterns depending on the beam shapes. Therefore, it is possible that additional material is made available behind the keyhole that can keep the keyhole stable for longer than the sole geometrical calculation predicted. This can explain the comparably high gap bridgability of beam shapes D, E, F and G.

Conclusions

According to the analytical model calculations, the melt pool width and gap width are the dominant factors defining the static geometry of the melt pool behind the keyhole. Surface tension and the material availability in the melt pool define the melt pool shape and the gap bridgability. Additional material can be made available and avoid a keyhole collapse by directed melt flows inside the melt pool.

Authors' Contributions Not applicable.

Funding The author kindly acknowledges the funding of SMART – Surface tension of Metals Above vapoRization Temperature (Vetenskapsrådet - The Swedish Research Council, 2020–04250) and Steel-S4EV – STEEL Solutions for Safe and Smart Structures of Electric Vehicles (EC Research Fund for Coal and Steel, RFCS, no. 800726). Open access funding provided by Lulea University of Technology.

Data Availability The datasets generated during the current study are available from the corresponding author on request.

Declarations

Competing interests The author has no relevant financial or non-financial interests to disclose.

Ethical approval Not applicable.

Open Access This article is licensed under a Creative Commons Attribution 4.0 International License, which permits use, sharing, adaptation, distribution and reproduction in any medium or format, as long as you give appropriate credit to the original author(s) and the source, provide a link to the Creative Commons licence, and indicate if changes were made. The images or other third party material in this article are included in the article's Creative Commons licence, unless indicated otherwise in a credit line to the material. If material is not included in the article's Creative Commons licence and your intended use is not permitted by statutory regulation or exceeds the permitted use, you will need to obtain permission directly from the copyright holder. To view a copy of this licence, visit <http://creativecommons.org/licenses/by/4.0/>.

References

1. Zhang, Y.M., Zhang, S.B.: Double-sided arc welding increases weld joint penetration. *Weld. Journal-Including Weld. Res. Supplement.* **77**(6), 57–62 (1998)
2. Hackmair, C., Werner, E., Pönisch, M.: Application of welding simulation for chassis components within the development of manufacturing methods. *Comput. Mater. Sci.* **28**(3–4), 540–547 (2003)
3. Cao, X., Wallace, W., Poon, C., Immarijeon, J.P.: Research and progress in laser welding of wrought aluminum alloys. I. Laser welding processes. *Mater. Manuf. Processes.* **18**(1), 1–22 (2003)
4. Wu, Q., Gong, J., Chen, G., Xu, L.: Research on laser welding of vehicle body. *Opt. Laser Technol.* **40**(2), 420–426 (2008)
5. Schultz, V., Seefeld, T., Vollertsen, F.: Gap bridging ability in laser beam welding of thin aluminum sheets. *Phys. Procedia.* **56**, 545–553 (2014)
6. Laskin, A., Laskin, V.: Variable beam shaping with using the same field mapping refractive beam shaper. In: *Laser Resonators, Microresonators, and Beam Control XIV*, vol. 8236, pp. 81–90. SPIE (2012, February)

7. Hagino, H., Shimizu, S., Ando, H., Kikuta, H.: Design of a computer-generated hologram for obtaining a uniform hardened profile by laser transformation hardening with a high-power diode laser. *Precis. Eng.* **34**(3), 446–452 (2010)
8. Dewi, H.S., Fischer, A., Volpp, J., Niendorf, T., Kaplan, A.F.: Microstructure and mechanical properties of laser surface treated 44MnSiVS6 microalloyed steel. *Opt. Laser Technol.* **127**, 106139 (2020)
9. Fetzer, F., Jarwitz, M., Stritt, P., Weber, R., Graf, T.: Fine-tuned remote laser welding of aluminum to copper with local beam oscillation. *Phys. Procedia.* **83**, 455–462 (2016)
10. Möbus, M., Woizeschke, P.: Laser beam welding setup for the coaxial combination of two laser beams to vary the intensity distribution. *Weld. World.* **66**(3), 471–480 (2022)
11. Volpp, J.: Formation mechanisms of pores and spatters during laser deep penetration welding. *J. Laser Appl.* **30**(1), 012002 (2018)
12. Volpp, J., Vollertsen, F.: Impact of multi-focus beam shaping on the process stability. *Opt. Laser Technol.* **112**, 278–283 (2019)
13. Volpp, J., Srowig, J., Vollertsen, F.: Spatters during laser deep penetration welding with a bifocal optic. In: *Advanced Materials Research*, vol. 1140, pp. 123–129. Trans Tech Publications Ltd (2016)
14. Volpp, J.: Multispot laser welding for increased gap bridgability. *J. Laser Appl.* **34**(4), 042002 (2022)
15. Laskin, A., Volpp, J., Laskin, V., Nara, T., Jung, S.R.: Multispot optics for beam shaping of high-power single-mode and multimode lasers. *J. Laser Appl.* **33**(4), 042046 (2021)
16. Cho, J.H., Na, S.J.: Implementation of real-time multiple reflection and fresnel absorption of laser beam in keyhole. *J. Phys. D.* **39**(24), 5372 (2006)
17. Fuhrich, T., Berger, P., Hügel, H.: Marangoni effect in laser deep penetration welding of steel. *J. Laser Appl.* **13**(5), 178–186 (2001)
18. Geiger, M., Leitz, K.H., Koch, H., Otto, A.: A 3D transient model of keyhole and melt pool dynamics in laser beam welding applied to the joining of zinc coated sheets. *Prod. Eng. Res. Devel.* **3**, 127–136 (2009)
19. Volpp, J.: Keyhole stability during laser welding—part II: Process pores and spatters. *Prod. Eng. Res. Devel.* **11**, 9–18 (2017)

Publisher's Note Springer Nature remains neutral with regard to jurisdictional claims in published maps and institutional affiliations.

Springer Nature or its licensor (e.g. a society or other partner) holds exclusive rights to this article under a publishing agreement with the author(s) or other rightsholder(s); author self-archiving of the accepted manuscript version of this article is solely governed by the terms of such publishing agreement and applicable law.